

Size and fluorescence measurements of individual droplets by flow cytometry

Jacques Fattaccioli,^{a*} Jean Baudry,^a Jean-Daniel Émerard,^a Emanuel Bertrand,^a Cécile Goubault,^a Nelly Henry^b and Jérôme Bibette^a

Received 28th August 2008, Accepted 20th February 2009
First published as an Advance Article on the web 30th April 2009
DOI: 10.1039/b814954b

Biotechnological applications of emulsions, such as micro-reactors or drug carriers, demand accurate characterization techniques, able to measure the size and biochemical content of the droplets at the individual level. Since no available characterization technique completely fulfills these needs, we extended the use of flow cytometry, which was originally developed for cell studies, to the straightforward and quantitative characterization of micron-sized emulsions. Our method determines the size of soybean oil droplets from flow cytometric measurements of forward scattering and side scattering intensities combined with the theoretical scattered intensities exactly derived from Mie theory and numerically integrated with respect to the optical setup of the instrument. We evaluate the accuracy of our method by comparing the size distribution obtained for a monodisperse emulsion sample to the corresponding distribution measured with a commercial instrument. Applied to emulsion droplets functionalized with fluorescent streptavidin, our method allows for monitoring of the rate of grafted molecules on interfaces with a precision never obtained before.

Introduction

In the past decades, a wide range of sophisticated colloids has been developed with biotechnological purposes. Probes for immunoassays,¹ contrast agents for biomedical imaging,² cell sorting auxiliaries,³ the list of potential applications of colloids is continuously increasing thanks to the great versatility of their physico-chemical nature (liquid,⁴ polymer,⁵ magnetic,⁶ core-shell,⁷ etc.) and to the possibility of modifying their surface properties through functionalization or surfactant adsorption.^{8,9} Although solid particles remain the most used, liquid particles such as liposomes¹⁰ and emulsions¹¹ recently joined the family of colloidal dispersions involved in biotechnological applications. They offer an even greater versatility than solid colloids since they can also encapsulate and transport biomolecules¹² or functional nanoparticles.¹³ While solid suspensions can be perfectly monodisperse thanks to the ordinarily used nucleation-growth synthesis,⁵ liquid suspensions are more often obtained by the fragmentation of a bulk phase in another^{14,15} and intrinsically show a broader size distribution. The small processed volumes and the difficulty in applying a controlled shearing in these conditions accentuate this tendency.

A number of techniques has been developed in order to measure the size distribution of colloidal dispersions.^{16,17} Most of them deduce the size distribution from the measurement of a bulk physical parameter such as the light scattered by the particles all together. Besides, the characterization of the density of biomolecules attached to or entrapped within the particles is very often done by fluorimetry or colorimetry¹⁸ on the entire

population of objects. All these methods are less accurate if the size distribution broadens,¹⁹ and, even in the case of techniques coupled with a separation device, such as field flow fractionation (FFF),²⁰ the level of characterization is always well below what is needed for interpreting experiments based on the characteristics of individual particles.²¹

Flow cytometry is a technique for counting, examining and sorting microscopic particles suspended in a stream of fluid. It allows simultaneous analysis of the physical and/or chemical characteristics of single cells flowing through an optical and/or electronic detection apparatus.²¹ This technology has applications in a great number of fields, including hematology, molecular biology, immunology and marine biology. In the field of molecular biology, it is especially useful when used with fluorescence tagged antibodies. These specific antibodies bind to antigens on the studied target cells and enable information on specific characteristics of the considered cells to be obtained. Modern flow cytometers are able to analyze several thousand particles per second, and can separate particles following precise scattering or fluorescence criteria. A flow cytometer is similar to a microscope, except that, instead of producing an image of the cell, it produces high-throughput automated quantification of set parameters.

In this article, we show that it is possible to use the light scattering signal in a quantitative way when dealing with oil-in-water emulsions. A simple numerical analysis allows simulation of the experimental scattering diagrams, the size of each droplet individually to be obtained and finally the whole size distribution of the emulsion sample to be built. As an illustration, we apply our technique to the characterization of streptavidin-functionalized emulsion droplets²² and show that the simultaneous recording of both the fluorescence and the size enables us to go well beyond the existing techniques.

^aLCMD - CNRS, UPMC, ESPCI, 10, rue Vauquelin, 75231 Paris Cedex 05, France

^bLaboratoires de Physico-Chimie, Institut Curie, CNRS UMR 168, Paris F-75005, France

Experimental section

Fabrication of the monodisperse emulsion

We disperse soybean oil (*Sigma-Aldrich*) at a fraction $\phi = 75\%$ w/w by gently stirring it in an aqueous phase comprised of 15%w/w of Poloxamer 188 block-polymeric surfactants ($\text{HO}(\text{C}_2\text{H}_4\text{O})_{79}(-\text{C}_3\text{H}_6\text{O})_{28}(\text{C}_2\text{H}_4\text{O})_{79}\text{H}$, *Uniqema*) and 2%w/w of sodium alginate (*Sigma-Aldrich*) used as a thickening agent. In order to get monodisperse droplets, we further shear this crude polydisperse emulsion in a Couette cell apparatus under a controlled shear rate of 5000 s^{-1} , following the method developed by Mason and Bibette.¹⁵ After fragmentation, the final diameter of the droplets is equal to $5 \pm 1 \mu\text{m}$.

Nile Red colored droplets. Nile Red is a lipophilic and solvatochromic fluorophore²³ characterized by a broad range of excitation and emission wavelengths. Prior to making the polydisperse emulsion sample, we dilute it in soybean oil at a concentration of $10^{-4} \text{ mol L}^{-1}$. We checked that at this concentration the fluorescence intensity of the Nile Red is not affected by any quenching effect.

Streptavidin-functionalized droplets. Soybean oil contains some free acidic molecules,²⁴ from the oleic acid family, which at neutral pH become surface active, making it possible to functionalize the carboxylic groups with compounds bearing a NH_2 moiety via the formation of a peptidic bond.⁸ We choose first to graft a biotin-derivative, biotin-($\text{C}_2\text{H}_4\text{O})_3-\text{NH}_2$ ($\text{C}_{16}\text{H}_{30}\text{N}_4\text{SO}_4$, *Interchim*), and then to bind fluorescent streptavidin to the biotins. **Biotin attachment:** The first step relies on the attachment of a small amino-biotin derivative to the carboxylic groups, which is activated by a carbodiimide coupling agent and a stabilizer. (i) **Activation of the carboxylic groups:** We dilute 17 μL of emulsion in a phosphate-Tween20 (PB-Tween20) buffer in a 500 μL microtube to obtain 200 μL of a suspension at $\phi = 5\%$ w/w. The PB-Tween20 buffer has an ionic strength of 20 mM, a pH = 7.3 and contains 0.2%w/w (~3CMC) Tween20 surfactant (mono-9-octadecanoate poly(oxy-1,2-ethanediyl), *Sigma-Aldrich*). The suspension is then gently mixed over 30 minutes with 50 μL of the activation solution containing 30 mg of EDAC (N-ethyl-N'-(3-dimethylaminopropyl)-carbodiimide hydrochloride, *Sigma-Aldrich*) and 5 mg of sNHS (sulfo,N-hydroxysuccinimide, *Sigma-Aldrich*) in the PB-Tween20 buffer. At the end of this reaction, we wash the suspension by removing 230 μL of the continuous phase and adding 180 μL of PB-Tween20. (ii) **Amino-biotin linkage:** 50 μL of a solution of biotin-($\text{C}_2\text{H}_4\text{O})_3-\text{NH}_2$ (*Interchim*) in PB-Tween20 at a concentration C_{biot} is added to the activated suspension and the tube content is slowly mixed for 30 minutes. C_{biot} ranges between 1 and 6 mg/mL in a PB-Tween20 buffer. At the end of the reaction, we wash the suspension 8 times with the PB-Tween20 buffer in order to remove the free amino-biotin molecules from the solution. **Streptavidin adsorption:** we complex fluorescein isothiocyanate (FITC)-conjugated streptavidin (*Interchim*) onto the biotin molecule so that the excitation and emission wavelength of the dye match with the laser wavelength of the flow cytometer. In a 500 μL microtube, we rinse 10 μL of the biotinylated emulsion with a MES-Tween20 buffer. This buffer has a MES concentration (2-(N-morpholino)ethanesulfonic acid, *Sigma-Aldrich*) of

20 mM, a pH = 5.3 and a Tween20 concentration of 0.2%w/w. Then, we mix the suspension for 15 minutes with 5 μL of the streptavidin solution ($C_{\text{Strep}} = 0.1 \text{ mg/mL}$ in a MES-Tween20 buffer) and 25 μL of MES-Tween20 buffer.

Measurements with the flow cytometer

For this study, we use a commercial Becton Dickinson FACSCalibur instrument linked to the software CellQuest Pro for analysis. The refractive indexes of soybean oil and PBS at the illumination wavelength (488nm) are respectively equal to $n_{\text{oil}} = 1.475 \pm 0.005$ and $n_{\text{PBS}} = 1.335 \pm 0.005$. Prior to each analysis, we dilute a small volume of the emulsion droplets in a PBS buffer in order to decrease the droplet concentration down to frequencies between 100 and 200 events per second.

In the instrument, a monochromatic laser beam (Argon, $\lambda = 488 \text{ nm}$) is directed onto a hydro-dynamically focused stream of fluid where the droplets circulate. Each suspended droplet passing through the beam scatters the light in some way, and fluorescent chemicals found in the particle or attached to the particle may be excited into emitting light at a higher wavelength than the light source. The detectors pick up this combination of scattered and fluorescent light, and by analyzing fluctuations in brightness on each detector it is possible to extrapolate various types of information about the physical and chemical structure of each individual particle.

A schematic top-view of the optical setup of the instrument is shown on Fig. 1: (i) the forward scattering intensity I_{FS} is recorded by a photodiode detector aligned with the laser beam; (ii) the side scattering intensity I_{SS} is collected perpendicularly to the laser beam by an high numerical aperture optical lens (n.a. = 1.2), filtered through a 90/10 Brewster angle beam splitter and

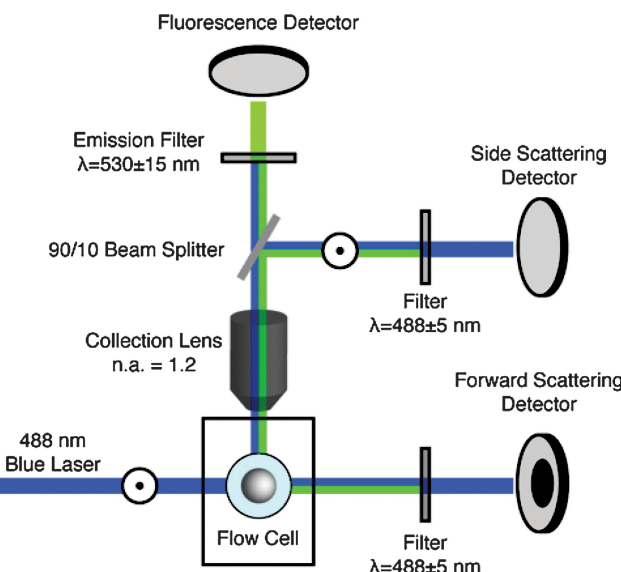


Fig. 1 Simplified schematic top-view of the BD FACScalibur instrument. An argon laser, linearly polarized along the flow direction, illuminates the particle suspended in the fluid. The forward scattered light is filtered and measured by a photodiode located in the incident beam direction. The side scattered and the fluorescence lights are collected through an high numerical aperture lens located perpendicularly to the incident direction.

recorded by a photomultiplier detector; (iii) the fluorescence intensity I_F emitted by the particles is also collected by the optical lens, and filtered in order to measure only the intensity relative to the wavelength of the fluorescent species attached to particles. The software normalizes the scattering and fluorescence intensities on 1024 bins.

Analytical expression of the scattered light intensities

When a spherical particle of radius r_D and refractive index n is illuminated by an electromagnetic wave $\vec{E}_i e^{i(kx-\omega t)}$ of wavelength λ and pulsation ω propagating along the z direction (Fig. 2), the relationship between the incident light $\vec{E}_i \begin{pmatrix} E_{//i} \\ E_{\perp i} \end{pmatrix}$ and the scattered light $\vec{E}_s \begin{pmatrix} E_{//s} \\ E_{\perp s} \end{pmatrix}$ in the local referential along the scattering direction is²⁵

$$\begin{pmatrix} E_{//s} \\ E_{\perp s} \end{pmatrix} = \frac{e^{i(k(r-z))}}{-ikr} \begin{pmatrix} S_2 & 0 \\ 0 & S_1 \end{pmatrix} \begin{pmatrix} E_{//i} \\ E_{\perp i} \end{pmatrix}$$

The scalars $E_{//}$ and E_{\perp} are the light components parallel and perpendicular to the scattering plane, respectively. The parameters S_1 and S_2 depend on the laser wavelength λ , the radius of the spherical particle r_D and the refractive index ratio n_{PBS}/n_{oil} . In the local referential $(\vec{e}_{//s}, \vec{e}_{\perp s})$, this expression becomes

$$\vec{E}_s = \frac{e^{i(k(r-z))}}{-ikr} \vec{X} \vec{E}_i$$

with

$$\vec{X} = (S_2 \cos\phi) \vec{e}_{//s} + (S_1 \sin\phi) \vec{e}_{\perp s}$$

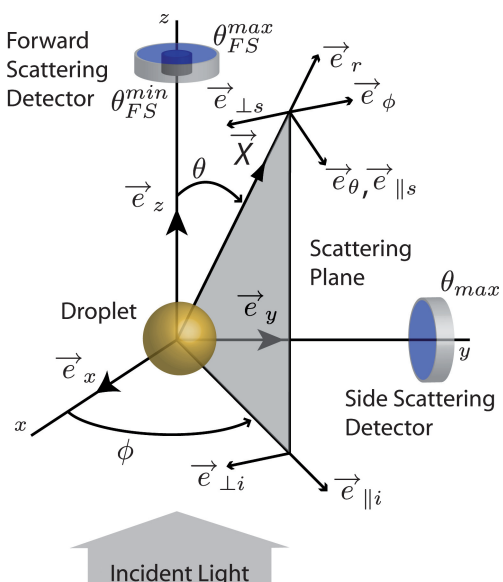


Fig. 2 Schematic representation of the geometric parameters used to compute the scattering intensity of an emulsion droplet illuminated by a laser beam. The forward detector is located along the z -axis and is defined by two angles associated to its aperture and the obscuration blade. The side detector is located along the y -axis.

Forward scattering intensity. An obscuration blade and the aperture of the optical components limit the forward scatter radiation impacting the detector to a half-cone angle cross-section ranging roughly from $\theta_{FS}^{\min} \approx 0.7$ to $\theta_{FS}^{\max} = 10$ degrees, following the specifications of the manufacturer. In the case of the forward detector, the z -axis is an axis of symmetry and the forward scattered intensity can be written:

$$I_{FS} = \frac{2\pi\alpha_{FS}}{k^2} \int_{\theta_{FS}^{\min}}^{\theta_{FS}^{\max}} \frac{1}{2} \left(|S_1|^2 + |S_2|^2 \right) \sin\theta d\theta$$

The scalar α_{FS} is introduced in order to take the power of the laser beam and the gain setup of the detector into account in the numerical computations.

Side scattering intensity. In order to increase the sensitivity of the instrument on the side scattering channel, the laser beam is polarized parallel to the fluid flow. The role of the Brewster angle beam on the back of the lens is to allow solely the scattered component parallel to \vec{e}_x to be measured. Under these conditions, only the term $|\vec{X} \cdot \vec{e}_x|^2$ is to be considered and can be written as

$$|\vec{X} \cdot \vec{e}_x|^2 = |S_2|^2 \cos^4\phi \cos^2\theta + |S_1|^2 \sin^4\phi + (S_2 S_1^* + S_1^* S_2) \cos^2\phi \sin^2\phi \cos\theta$$

The side scattered light is collected through an optical lens of high numerical aperture, imposing a circular cross-section limited by the optical aperture θ_{SS}^{\max} of the lens on the integration of the elementary signal.

The angular spherical variables (θ, ϕ) are not independent in this case and their relationship can be expressed as:

$$\phi = \arcsin\left(\frac{\sin\theta_{SS}^{\max}}{\sin\theta}\right)$$

If we introduce a scalar parameter α_{SS} analogous to α_{FS} , the side scattered intensity becomes

$$I_{SS} = \frac{\alpha_{SS}}{k^2} \int_{\frac{\pi}{2}-\theta_{SS}}^{\frac{\pi}{2}+\theta_{SS}} \int_{\frac{\pi}{2}-\phi(\theta)}^{\frac{\pi}{2}+\phi(\theta)} |\vec{X} \cdot \vec{e}_x|^2 \sin\theta d\theta d\phi$$

The aperture angles θ_{FS}^{\min} and θ_{FS}^{\max} depend on each instrument and are adjusted by the manufacturer to assure standard results at the end of the fabrication process. We were unable to obtain their precise values for our instrument from the manufacturer, neither to measure them directly. Similarly the values of α_{FS} and α_{SS} were unknown since we were unable to determine the exact conversion rate between the collected light and the output signals performed by the detectors and the amplifiers. Keeping in mind that we used these as four adjustable parameters, we will not discuss them any further since they show no strong significance and depend on the daily setup of the instrument.

Numerical computation of the scattered signals

The Mie theory formalism and the referential descriptions are those introduced by Bohren and Huffman.²⁵ All the simulations of the scattered intensities were performed with Mathworks Matlab numerical routines created by Mätzler.²⁶

Results and discussion

On Fig. 3, we superimposed the scattering diagrams $I_{SS}(I_{FS})$ obtained from a polydisperse (red) and a monodisperse (blue) soybean oil emulsion sample. These diagrams are built from the superposition of the scattering intensities I_{FS} and I_{SS} collected for $M = 10\,000$ droplets crossing the illumination beam one by one. Although the diagram corresponding to the monodisperse sample has a narrower extension than the one of the polydisperse sample, the red and blue $I_{SS}(I_{FS})$ curves have the same shape and overlay each other perfectly. Intuitively, the extension of the curve is related to the size distribution of the emulsion sample.

Numerical adjustment of the experimental scattering diagrams

According to the integral expressions of the forward and side scattering intensities we detailed in the Experimental section, the

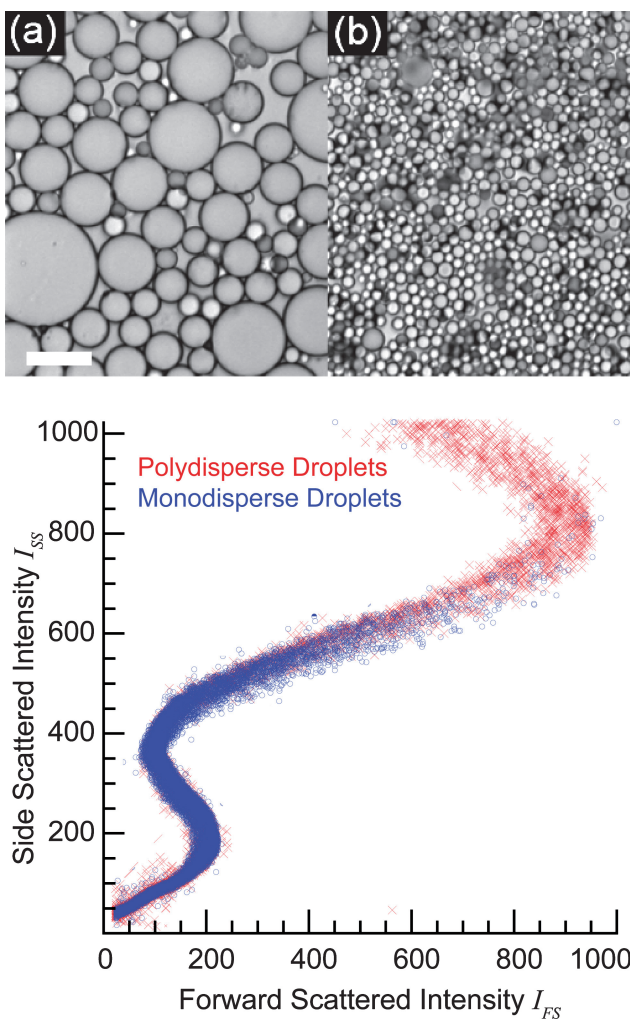


Fig. 3 (Top) Pictures of the polydisperse (a) and the monodisperse (b) soybean oil emulsion samples. The monodisperse sample has a mean diameter close to $5 \pm 1 \mu\text{m}$ (scalebar $20 \mu\text{m}$). (Bottom) Superposition of the scattering diagrams $I_{SS}(I_{FS})$ for the polydisperse (red) and the monodisperse (blue). The scattering diagrams share the same profile but the diagram corresponding to the monodisperse sample has a narrower extension than the polydisperse diagram. The instrument setup does not allow the scattering intensities relative to the biggest droplets of the polydisperse sample, which can range up to $30 \mu\text{m}$, to be seen.

simulation of the scattering data requires the refractive index ratio of the particles, their sizes, the aperture angles of the forward detector and some gain parameters as input. As compared to other published works using the flow cytometer as a size measuring technique,^{27–29} emulsions constitute an ideal material for the simulation of the scattered signals thanks to their spherical shapes and their continuously distributed sizes. Moreover, we are able to create emulsion samples containing solely separated individual droplets without any multiplets. As a consequence, the analytical expressions of the scattered intensity can thus be applied numerically without any assumption since Mie theory is exact in the case of homogeneous individual spherical objects

In order to fit the experimental diagram composed of M data indexed as $\{A_j\}_{j=1\dots M} = (I_{FS,j}^{meas}, I_{SS,j}^{meas})_{j=1\dots M}$, we consider a set of $N = 1000$ spherical droplets with radii ranging between $r_D = 0.250 \mu\text{m}$ and $4.250 \mu\text{m}$ and with a refractive index n_{oil} , for which we calculate numerically their scattering intensities $\{B_i\}_{i=1\dots N} = (I_{FS,i}^h, I_{SS,i}^h)_{i=1\dots N}$.

In order to properly fit the scattering diagrams we measure, we adjust the theoretical set of points $\{B_i\}_{i=1\dots N}$ to the experimental set $\{A_j\}_{j=1\dots M}$ with respect to the aperture angles θ_{FS}^{\min} and θ_{FS}^{\max} and the gain parameters α_{FS} and α_{SS} we introduced in the Experimental section. We also consider the refractive index of the oil n_{oil} as a fifth adjustable parameter since it appeared that the numerical method was very sensitive to its value. The numerical distance D between the measured and the fitted curves is the sum of the elementary distances $d_j(A_j, B_i)$ between each experimental point A_j and its closest computed point B_i :

$$D = \sum_{j=1}^M d_j(A_j, B_i)$$

where $d_j(A_j, B_i) = \min((I_{FS,i}^h - I_{FS,j}^{meas})^2 + (I_{SS,i}^h - I_{SS,j}^{meas})^2) i = 1\dots N$.

We obtain the best adjustment by minimizing, through a Simplex method,³⁰ the total distance $D = \sum_{j=i}^M d_j(A_j, B_i)$ with respect to the five optical and instrumental independent parameters. The boundary conditions ($\theta_{FS}^{\min} = 0.7^\circ$, $\theta_{FS}^{\max} = 10^\circ$, $n_{oil} = 1.475$) for the numerical minimization of the parameter D are imposed by the measurement of the refractive index of the soybean oil and by the manufacturer specifications of the FACSCalibur cytometer. We obtain the best simulation with the following set of parameters: $\theta_{FS}^{\min} = 0.716^\circ$, $\theta_{FS}^{\max} = 3.954^\circ$ and $n_{oil} = 1.468$.

The optimized parameters are in excellent agreement with the manufacturer specifications and the allowable variability on the refractive index of the oil. Fig. 4 (left) shows the resulting I_{FS} and I_{SS} intensities as a function of a droplet radius r_D ranging from 0.250 to $4.250 \mu\text{m}$. The shape of the scattering diagrams for soybean oil emulsions originates from the oscillating behavior of the forward scattering intensity I_{FS} , whereas the side scattering intensity I_{SS} increases monotonically with respect to the size of the droplets. It is interesting to note that on the contrary to these results, when dealing with cells or particles with a refractive index ratio close to one, the forward scattering intensity is read as proportional to the volume of the particles whereas the side scattering intensity depends on the cell structure, *i.e.* the shape of the nucleus, the amount and type of cytoplasmic granules or the membrane roughness.³¹

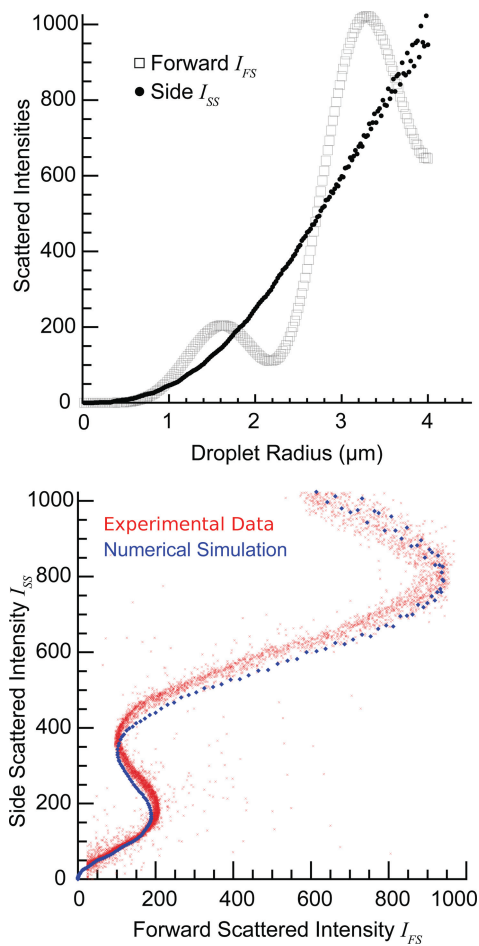


Fig. 4 (Top) Graphical representation of the numerical forward scattering intensity I_{FS} (□) and the side scattering intensity I_{SS} (●) as a function of the droplet radius. (Bottom) The simulation was performed with the following parameters: $0.716^\circ < \theta_{forward} < 3.954^\circ$ and $n_{oil} = 1.468$ after the minimization of the distance between the measured scattering diagram of the polydisperse sample (red) and the simulated I_{SS} (I_{FS}) curve (blue).

We report in Fig. 4 (right) the overlay of the measured scattering diagram (red) and the simulated curve (blue). The lateral broadening of the experimental curve as compared to the theoretical one is mainly due to the noise introduced by the light detection. Indeed, we observe that the increase of the flow rate noticeably broadens the scattering diagram.

The simulations are sensitive to the third decimal of the refractive index of the oil, which is very uncommon for light scattering measurements.¹⁹ Usually, defining the refractive indexes up to the second decimal is sufficient to perform a static light scattering measurement of the size distribution, but, in our study, we adjust the scattered signal upon all sizes of the sample.

Size distribution of a monodisperse emulsion sample

Statistically, when the flow cytometer measurement is performed on a wide enough population of particles, the percentage of droplets with a given radius r_D can be simply derived from the number of experimental dots which are in the close vicinity of the

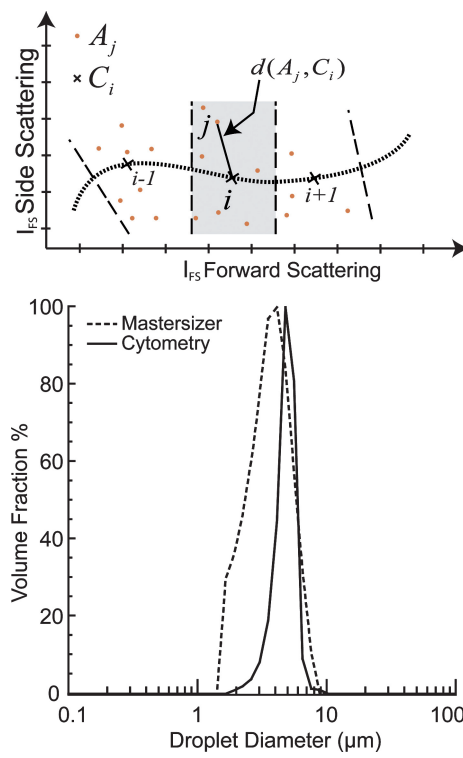


Fig. 5 (Top) Schematic representation of the numerical method used to build the size distribution of an emulsion sample from the simulation of the scattering diagram. (Bottom) Size distribution of a monodisperse emulsion measured with a Malvern Mastersizer S instrument (---) and with our numerical technique (—). The two distributions share the same mean values but the polydispersity is smaller when measured with the flow cytometer.

simulated datapoint $(I_{FS}(r_D), I_{SS}(r_D))$, as represented schematically on Fig. 5 (top).

On Fig. 5 (bottom) we superimposed the size distribution, expressed as a volume percentage, of a monodisperse emulsion obtained both through our simulation and with a commercial Malvern Mastersizer instrument.³² Although the two distributions have the same shape and the same average radius, our method gives a narrower distribution. The Malvern Mastersizer instrument records the average scattered light from a large number of objects at different angles. For a monodisperse sample, the relative intensity between detectors gives information on the size of the droplets, whereas the absolute intensity is related to the total number of objects. With a careful positioning of the detectors, sizes from 0.02 to 2000 μm can be measured. On the other hand, for polydisperse samples the Malvern instrument needs to assume *a priori* the supposed shape of the distribution (normal, monomodal, bimodal, etc.) in order to give the most probable size distribution corresponding to a mean measurement performed on the whole sample containing droplets with different sizes. As a consequence the same scattered light signal¹⁹ can be interpreted as different size distributions since the non-monotonic behavior of the scattered light with respect to the size of the particles usually leads to an over- or under-estimation of certain subpopulations of droplets within the sample. With the cytometer, measuring the objects one by one allows us to determine the absolute distributions precisely without any assumptions. On the

other hand, the scattering signal is always measured with the same detectors whatever the size, so measurements have limited dynamics. Other one by one methods, like the Coulter Counter face the same limitation. A typical recording, as shown in Fig. 3 (bottom), displays beads droplets with radii ranging from 0.8 to 4.5 μm . By adjusting the detector's gain, it is still possible to broaden the accessible range, from typically 500 nm to 10 μm in radii. For smaller droplets, the scattering signal is very low, so the measurement becomes very noisy. For larger droplets, our analysis seems less valid, perhaps due to some deformation of the droplet in the flow.

Validation of the simultaneous fluorescence and size characterizations

In the case of the polydisperse emulsion sample tainted by Nile Red, the fluorescence of each droplet is proportional to its volume since the dye is non soluble in water. Since the flow cytometer records the fluorescence intensity I_F and its radius r_D for each droplet thanks to our numerical method, we can plot $I_F(r_D^3)$ as is shown in Fig. 6. As expected the fluorescence intensity increases linearly with the volume of the droplets over the whole range of measurement.

Characterization of streptavidin-functionalized emulsion droplets²²

Following the chemical process reported in the Experimental section, we are able to functionalize the surface of soybean oil droplets with fluorescent streptavidins bearing 8 to 12 FITC moieties each. We convert the fluorescence intensity I_F of each particle in a number of FITC molecules and streptavidins N_{Strep} per droplet using a fluorescence calibration kit provided by Bangs Laboratories (Quantum FITC MESF High Level). Since we independently measured the size of each droplet, we can plot in Fig. 7 (top) the intensity of fluorescence of each droplet as a function of the droplet surface $S = 4\pi r_D^2$ and in

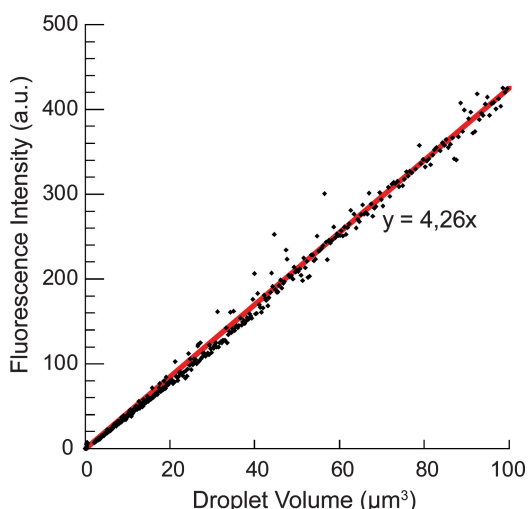


Fig. 6 Evolution of the fluorescence intensity of soybean emulsion droplets encapsulating an amount of Nile Red molecules. The intensity increases linearly with respect to the volume of the droplets.

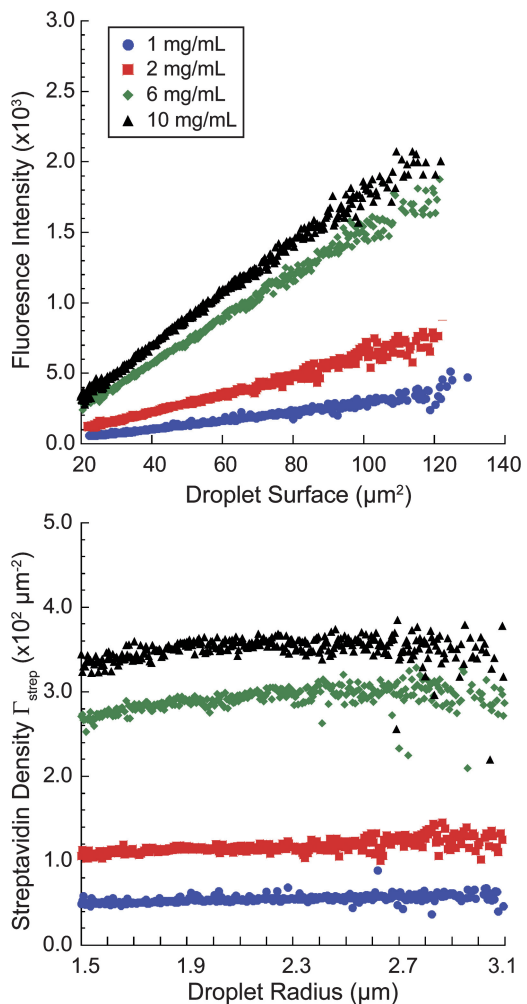


Fig. 7 (Top) Intensity of fluorescence of functionalized droplets plotted as a function of their surface area, for four conditions of increasing amino-modified biotin concentrations. The fluorescence increases linearly for all conditions. (Bottom) Density of streptavidins per droplet Γ_{Strep} plotted as a function of the droplet radius r_D .

Fig. 7(bottom) the density of streptavidins per droplet $\Gamma_{\text{Strep}} = \frac{N_{\text{Strep}}}{4\pi r_D^2}$ as a function of the droplet radius r_D for four functionalization conditions of amino-biotin. All four emulsions were mixed with the same streptavidin solution, with an excess of streptavidin as compared to the biotin available on the surface. The streptavidin density curves $\Gamma_{\text{Strep}}(r_D)$ are essentially constant with respect to the radius of the droplets since streptavidins are grafted solely on the surface of the droplets. Streptavidin has a molecular surface area³³ close to 30 nm^2 , therefore the streptavidin densities used here correspond to roughly 1% of a theoretical full monolayer coverage. These densities are proportional to the amount of amino-biotin introduced, except for the largest case. In this latter case, we hypothesize that the yield of peptide bond formation is decreasing, due to limited amount of free acidic molecules in the soybean oil. We have also checked the absence of fluorescence signal in the absence of amino-biotin.

Conclusion

In this article, we exposed a novel emulsion characterization method built on the numerical simulation of the forward and side scattering intensities recorded by a flow cytometer. Starting from the Mie theory and from the optical setup of the instrument, we wrote the integral expressions of the scattered intensities as a function of the refractive index ratio, the size of the droplets, the aperture angles of the forward detector and of some gain parameters. The forward scattering and side scattering intensities were efficiently simulated and the corresponding optimized parameters were found to be in agreement with both the manufacturer specifications and the tolerance on the refractive index measurements. The shape of the experimental scattering diagram was attributed to the non-monotonic behavior of the forward-scattering intensity, while the side scattering intensity increases monotonically with respect to the size of the droplets.

The flow cytometer allowed measurement of the size of the droplets individually, hence building the size distribution of a monodisperse emulsion sample without any hypothesis on its shape. To this extent, and in the size range where it can be applied, typically for droplet radii in the 0.5 to 10 μm range, our method is much more accurate than any commercial size characterization technique. When used for the study of fluorescent droplets, the flow cytometer allowed the fluorescence intensity of each particle to be plotted with respect to its size. We first validated this approach on oil droplets colored with a lipophilic dye and we showed that the fluorescence intensity scaled with the volume of the droplets. The method we presented here is, to our knowledge, the only one that allows straightforward characterization of the size and the biomolecule content of individual emulsion droplets, without the need for a monodisperse size distribution.

References

- 1 J. Baudry, C. Rouzeau, C. Goubault, C. Robic, L. Cohen-Tannoudji, A. Koenig, E. Bertrand and J. Bibette, *Proceedings of the National Academy of Sciences of the United States of America*, 2006, **103**, 16076–16078.
- 2 P. Caravan, J. J. Ellison, T. J. McMurry and R. B. Lauffer, *Chemical Reviews*, 1999, **99**, 2293–2352.
- 3 Q. A. Pankhurst, J. Connolly, S. K. Jones and J. Dobson, *Journal of Physics D - Applied Physics*, 2003, **36**, R167–R181.
- 4 G. M. Lanza, K. D. Wallace, M. J. Scott, W. P. Cacheris, D. R. Abendschein, D. H. Christy, A. M. Sharkey, J. G. Miller, P. J. Gaffney and S. A. Wickline, *Circulation*, 1996, **94**, 3334–3340.
- 5 J. Ugelstad, A. Berge, T. Ellingsen, R. Schmid, T. N. Nilsen, P. C. Mork, P. Stenstad, E. Hornes and O. Olsvik, *Progress in Polymer Science*, 1992, **17**, 87–161.
- 6 J. Bibette, *Journal of Magnetism and Magnetic Materials*, 1993, **122**, 37–41.
- 7 W. C. W. Chan and S. M. Nie, *Science*, 1998, **281**, 2016–2018.
- 8 G. Hermanson, *Bioconjugate Techniques*, Academic Press, 1996.
- 9 J. Israelachvili, *Intermolecular and Surface Forces*, Academic Press, 1992.
- 10 W. T. Al-Jamal and K. Kostarelos, *International Journal of Pharmaceutics*, 2007, **331**, 182–185.
- 11 S. Benita and M. Y. Levy, *Journal of Pharmaceutical Sciences*, 1993, **82**, 1069–1079.
- 12 K. Bernath, M. T. Hai, E. Mastrobattista, A. D. Griffiths, S. Magdassi and D. S. Tawfik, *Analytical Biochemistry*, 2004, **325**, 151–157.
- 13 S. K. Mandal, N. Lequeux, B. Rotenberg, M. Tramier, J. Fattacioli, J. Bibette and B. Dubertret, *Langmuir*, 2005, **21**, 4175–4179.
- 14 R. C. Macdonald, R. I. Macdonald, B. P. M. Menco, K. Takeshita, N. K. Subbarao and L. R. Hu, *Biochimica Et Biophysica Acta*, 1991, **1061**, 297–303.
- 15 T. G. Mason and J. Bibette, *Langmuir*, 1997, **13**, 4600–4613.
- 16 A. Cao, *Analytical Letters*, 2003, **36**, 3185–3225.
- 17 CPS Instruments, <http://www.cpsinstruments.com/>.
- 18 P. K. Smith, R. I. Krohn, G. T. Hermanson, A. K. Mallia, F. H. Gartner, M. D. Provenzano, E. K. Fujimoto, N. M. Goede, B. J. Olson and D. C. Klenk, *Analytical Biochemistry*, 1985, **150**, 76–85.
- 19 W. Brown, *Dynamic Light Scattering: The Method and Some Applications*, Oxford Science Publications, Oxford, 1992.
- 20 M. Martin, *Advances in Chromatography*, 1998, **39**, 1–138.
- 21 H. M. Shapiro, in *Practical Flow Cytometry*, ed. Alan R. Liss, New York, 1985.
- 22 J. Fattacioli, J. Baudry, N. Henry, F. Brochard-Wyart and J. Bibette, *Soft Matter*, 2008, **4**, 2434–2440.
- 23 P. Greenspan, E. P. Mayer and S. D. Fowler, *Journal of Cell Biology*, 1985, **100**, 965–973.
- 24 J. Helme, *Soybean Oil Refining*, American Soybean Oil Association, Saint-Louis, MO, 1984.
- 25 C. F. Bohren and D. R. Huffman, *Absorption and Scattering of Light by Small Particles*, Wiley-Interscience, New York, 1983.
- 26 C. Mätzler, Mie Matlab Code, <http://diogenes.iwt.uni-bremen.de/vl/laser/codes/Mie-Matlab-Maetzler.zip>, 2002.
- 27 D. H. Tycko, M. H. Metz, E. A. Epstein and A. Grinbaum, *Appl. Optics*, 1985, **24**, 1355–1365.
- 28 S. G. Ackleson and R. W. Spinrad, *Appl. Optics*, 1988, **27**, 1270–1277.
- 29 R. E. Green, H. M. Sosik, R. J. Olson and M. D. DuRand, *Appl. Optics*, 2003, **42**, 526–541.
- 30 W. Press, B. P. Flannery, S. A. Teukolsky and W. T. Vetterling, *Numerical Recipes in C: The Art of Scientific Computing*, Cambridge University Press, 1992.
- 31 M. Hai, K. Bernath, D. Tawfik and S. Magdassi, *Langmuir*, 2004, **20**, 2081–2085.
- 32 Malvern Instruments, <http://www.malvern.com>.
- 33 S. Scheuring, D. J. Muller, P. Ringler, J. B. Heymann and A. Engel, *Journal of Microscopy*, 1999, **193**, 28–35.